

6 Serbestlik Dereceli Robotik Kolun Gelişmiş Simülasyon Teknikleriyle Kapsamlı Dinamik Analizi

Merdan ÖZKAHRAMAN*¹ 

¹Isparta Uygulamalı Bilimler Üniversitesi, Teknoloji Fakültesi, Mekatronik Mühendisliği Bölümü, 32260, Isparta, Türkiye

(Alınış / Received: 30.01.2025, Kabul / Accepted: 08.04.2025, Online Yayınlanma / Published Online: 25.04.2025)

Anahtar Kelimeler

Robotik kol,
Dinamik analiz,
Tork analizi,
Robotik eklem dinamiği

Öz: Bu makale, altı serbestlik derecesine (6-DOF) sahip bir robotik kolun MATLAB Simulink ortamında gelişmiş simülasyon teknikleri kullanılarak gerçekleştirilen ayrıntılı dinamik analizini sunmaktadır. Çalışma, robotik kolun eklem hareketleri, yörünge takibi, yük taşıma, bozucu etkilere karşı direnç ve dinamik ortamlarda gezinme gibi çeşitli çalışma koşulları altındaki performansını değerlendirmeye odaklanmaktadır. Kinematik ve dinamik modeller, Denavit-Hartenberg (D-H) parametreleri ve Lagrange denklemleri kullanılarak geliştirilmiş, böylece kolun hareket ve kuvvet etkileşimleri kapsamlı bir şekilde analiz edilmiştir. Eklem girişlerine farklı genliklerde sinüzoidal sinyaller uygulanmış ve açısal yer değiştirme, hız, ivme ve tork profilleri ayrıntılı biçimde elde edilmiştir. Bulgular, taban ekleminin daha geniş dönme hareketlerinden sorumlu olması nedeniyle en yüksek tork değerlerine maruz kaldığını, bilek eklemlerinin ise hassas kontrol için daha küçük ve sık ayarlamalar gerçekleştirdiğini ortaya koymaktadır. Çalışma, her bir eklemin kendine özgü taleplerine uygun kontrol stratejileri ve aktüatör tasarımlarının önemine vurgu yapmaktadır. Bu çalışma, endüstriyel ve araştırma uygulamalarında kullanılan 6-DOF robotik kollar için optimize edilmiş kontrol stratejileri ve verimli tahrik sistemlerinin geliştirilmesine yönelik değerli bir temel sunmaktadır.

Comprehensive Dynamic Analysis of a 6-DOF Robotic Arm Using Advanced Simulation Techniques

Keywords

Robotic arm,
Dynamic analysis,
Torque analysis,
Robotic joint dynamics

Abstract: This paper presents a detailed dynamic analysis of a six degrees of freedom (6-DOF) robotic arm using advanced simulation techniques in MATLAB Simulink. The study focuses on evaluating the robotic arm's performance under various operational conditions, including joint movements, trajectory tracking, payload handling, disturbance rejection, and navigation in dynamic environments. Kinematic and dynamic models were developed using the Denavit-Hartenberg (D-H) parameters and Lagrange equations, enabling a comprehensive understanding of the arm's motion and force interactions. Sinusoidal inputs with varying amplitudes were applied to the joints, producing detailed profiles for angular displacement, velocity, acceleration, and torque. The findings reveal that the base joint experiences the largest torques due to its role in broader rotational movements, while wrist joints exhibit smaller, more frequent adjustments required for precise control. The study emphasizes the importance of tailored control strategies and actuator designs to meet the unique demands of each joint. This study provides a valuable foundation for developing optimized control strategies and efficient actuation systems for 6-DOF robotic arms used in industrial and research applications.

1. Introduction

Robotic arms have become an indispensable tool in various industrial and research applications due to

their precision, versatility, and efficiency. They are extensively utilized in manufacturing, assembly, medical surgeries, and even space exploration. The capability of robotic arms to perform complex tasks with high accuracy and repeatability has revolutionized automation processes, leading to significant improvements in productivity and quality [1, 2]. In manufacturing, for example, robotic arms are used for welding, painting, and material handling, significantly reducing human error and increasing throughput. In the medical field, robotic-assisted surgeries allow for minimally invasive procedures with enhanced precision, reducing recovery times for patients [3, 4]. The dynamic analysis of robotic arms is a critical area of study that ensures their optimal performance and reliability. Understanding the dynamics of these systems is essential for designing control strategies that can handle the complex interactions between the joints and links of the robotic arm [5]. Previous research has explored various methodologies for analyzing the dynamics of robotic arms, including the use of Denavit-Hartenberg (D-H) parameters for kinematic modeling and Lagrange equations for dynamic modeling [6, 7]. These studies have laid the foundation for understanding the motion and force interactions within robotic systems, providing valuable insights into their design and control. Additionally, methods such as Newton-Euler formulations and virtual work principles have been employed to model and simulate the dynamic behavior of robotic arms, offering different perspectives and approaches to tackling the challenges in this field [8, 9].

Despite the progress made, the dynamic behavior of robotic arms, especially those with multiple degrees of freedom, remains a complex and challenging area of research. The interactions between various joints and the impact of external forces and torques need to be thoroughly understood to enhance the performance and safety of these systems [10-12]. Moreover, with the increasing demand for more sophisticated and adaptable robotic systems, there is a continuous need for advanced analytical and simulation techniques to address the evolving challenges.

This paper aims to build upon the existing body of knowledge by presenting a comprehensive dynamic analysis of a six degrees of freedom (6-DOF) robotic arm. Utilizing advanced simulation techniques, this study will derive and simulate the equations of motion, evaluate the performance of the robotic arm under different operational conditions, and present the torque requirements for each joint. The findings from this analysis will contribute to the development of more efficient and robust robotic arms, enhancing their application in various fields. Specifically, the paper will provide detailed torque graphs for each joint, highlighting the dynamic responses under varying loads and operational scenarios. These insights will be invaluable for engineers and

researchers working on the design and control of robotic systems, offering practical guidelines and benchmarks for future developments.

2. Mathematical Modeling

Mathematical modeling is a fundamental step in the analysis and design of robotic systems. For a six degrees of freedom (6-DOF) robotic arm, it involves creating a precise mathematical representation of the system's kinematics and dynamics. This representation is crucial for understanding how the robotic arm moves and responds to various inputs and forces. Accurate modeling ensures that simulations and control strategies developed later are effective and reliable.

The kinematic analysis focuses on the geometric relationships between different parts of the robotic arm. It involves defining the position, orientation, and motion of each link and joint in the system. This is typically achieved using the Denavit-Hartenberg (D-H) parameters, which provide a standardized method to describe the spatial configuration of robotic manipulators [13, 14]. By establishing the transformation matrices for each link, we can determine the position and orientation of the end-effector in the Cartesian space [15].

Dynamic modeling, on the other hand, deals with the forces and torques that cause motion in the robotic arm. It requires formulating the equations of motion that govern the behavior of the system under various operational conditions [16, 17]. The Lagrange equations are commonly used for this purpose, as they provide a systematic approach to derive these equations by considering the kinetic and potential energy of the system [18, 19]. Alternatively, Newton-Euler formulations can be applied to achieve the same goal, offering a different perspective on the dynamics of the robotic arm [20, 21].

In this section, we will first conduct a detailed kinematic analysis of the 6-DOF robotic arm, defining the D-H parameters and deriving the transformation matrices for each link. Following this, we will delve into the dynamic analysis, formulating the equations of motion using the Lagrange method. This comprehensive mathematical model will serve as the foundation for subsequent simulation and analysis, allowing us to evaluate the performance and control strategies of the robotic arm accurately.

2.1. Kinematic analysis

The robotic arm under consideration is designed with six degrees of freedom (6-DOF), enabling it to perform a wide range of movements and tasks. Each degree of freedom corresponds to a joint that provides either rotational or translational motion, allowing the end-effector to reach any position and orientation within

its workspace. The typical configuration of a 6-DOF robotic arm includes a combination of revolute and prismatic joints, although revolute joints are more common in most industrial applications. The six joints are usually arranged in a serial chain, starting from the base, which is fixed, to the end-effector, which interacts with the environment [22, 23]. The joints are labeled as follows:

- Base Joint (Joint 1): Rotational joint that allows the arm to rotate around the vertical axis.
- Shoulder Joint (Joint 2): Rotational joint that enables up-and-down movement of the arm.
- Elbow Joint (Joint 3): Rotational joint that allows the extension and retraction of the arm.
- Wrist Pitch Joint (Joint 4): Rotational joint that controls the pitch (up-and-down tilt) of the wrist.
- Wrist Yaw Joint (Joint 5): Rotational joint that controls the yaw (side-to-side rotation) of the wrist.
- Wrist Roll Joint (Joint 6): Rotational joint that controls the roll (twisting motion) of the wrist.

This configuration allows the end-effector to achieve a desired position and orientation in three-dimensional space, making the 6-DOF robotic arm highly versatile and suitable for complex tasks such as assembly, welding, and material handling.

The Denavit-Hartenberg (D-H) convention is a systematic method to describe the geometry of a robotic manipulator [24, 25]. It simplifies the kinematic equations by standardizing the notation for the link parameters [26, 27]. The D-H parameters consist of four values for each joint: link length a_{i-1} , link twist α_{i-1} , link offset d_i , and joint angle θ_i .

For a 6-DOF robotic arm, the D-H parameters are defined as follows:

- a_{i-1} : The distance between the axes of two consecutive joints along the common normal.
- α_{i-1} : The angle between the axes of two consecutive joints, measured along the common normal.
- d_i : The distance along the previous z-axis to the common normal.
- θ_i : The angle around the previous z-axis to the common normal.

Using these parameters, we can derive the transformation matrix ${}^{i-1}T_i$ for each link i , which represents the position and orientation of the link relative to the previous link [28, 29]. The transformation matrix ${}^{i-1}T_i$ is given by:

$${}^{i-1}T_i = \begin{bmatrix} c\theta_i & -s\theta_i & 0 & a_{i-1} \\ s\theta_i c\alpha_{i-1} & c\theta_i c\alpha_{i-1} & -s\alpha_{i-1} & -s\alpha_{i-1}d_i \\ s\theta_i s\alpha_{i-1} & c\theta_i s\alpha_{i-1} & c\alpha_{i-1} & c\alpha_{i-1}d_i \\ 0 & 0 & 0 & 1 \end{bmatrix}$$

By multiplying these individual transformation matrices (Eq. 1), we obtain the overall transformation matrix 0T from the base of the robotic arm to the end-effector:

$${}^0T = {}^0T_1 \cdot {}^1T_2 \cdot {}^2T_3 \cdot {}^3T_4 \cdot {}^4T_5 \cdot {}^5T_6 \quad (1)$$

This overall transformation matrix 0T describes the position and orientation of the end-effector in the Cartesian space, allowing us to perform the desired tasks with high precision. The kinematic analysis using D-H parameters thus provides a clear and efficient way to model the robotic arm's movements and capabilities.

2.2. Dynamic equations

The dynamic behavior of a robotic arm is governed by the forces and torques that act on its joints and links. To derive the dynamic equations, we use the Lagrange formulation, which provides a systematic approach to obtaining the equations of motion based on the energy of the system [19, 30-33]. The Lagrange formulation involves the following steps:

Kinetic Energy (T): The kinetic energy of the robotic arm is the sum of the kinetic energies of all its links. For each link i , the kinetic energy is given by:

$$T_i = \frac{1}{2} m_i v_i^T v_i + \frac{1}{2} \omega_i^T I_i \omega_i \quad (2)$$

where m_i is the mass of the link, v_i is the linear velocity of the center of mass of the link, ω_i is the angular velocity, and I_i is the inertia tensor of the link.

2. Potential Energy (V): The potential energy of the robotic arm is the sum of the potential energies of all its links, typically due to gravity. For each link i , the potential energy is given by:

$$V_i = m_i g h_i \quad (3)$$

where g is the acceleration due to gravity and h_i is the height of the center of mass of the link.

3. Lagrangian (L): The Lagrangian of the system is the difference between the total kinetic energy and the total potential energy:

$$L = T - V \quad (4)$$

4. Lagrange Equations of Motion: The equations of motion are obtained using the Lagrange equation:

$$\frac{d}{dt} \left(\frac{\partial L}{\partial \dot{q}_i} \right) - \left(\frac{\partial L}{\partial q_i} \right) = \tau_i \quad (5)$$

where q_i is the generalized coordinate (joint angle or displacement), \dot{q}_i is the generalized velocity, and τ_i is the generalized force (torque or force) acting on the joint.

By applying the Lagrange equations to each joint of the robotic arm, we can derive the equations of motion that describe the dynamics of the entire system.

The equations of motion for a 6-DOF robotic arm can be expressed in matrix form as:

$$M(q)\ddot{q} + C(q, \dot{q})\dot{q} + G(q) = \tau \quad (5)$$

where:

- $M(q)$ is the mass (inertia) matrix, representing the inertial properties of the robotic arm.
- $C(q, \dot{q})$ is the Coriolis and centrifugal matrix, accounting for the Coriolis and centrifugal forces.
- $G(q)$ is the gravity vector, representing the gravitational forces acting on the links.
- q is the vector of generalized coordinates (joint angles).
- \dot{q} is the vector of generalized velocities.
- \ddot{q} is the vector of generalized accelerations.
- τ is the vector of generalized forces (torques).

Each term in this equation can be detailed as follows:
Mass Matrix:

$$M(q) = \begin{bmatrix} m_{11} & m_{12} & \cdots & m_{16} \\ m_{21} & m_{22} & \cdots & m_{26} \\ \vdots & \vdots & \ddots & \vdots \\ m_{61} & m_{62} & \cdots & m_{66} \end{bmatrix}$$

Coriolis and Centrifugal Matrix:

$$C(q, \dot{q}) = \begin{bmatrix} c_{11} & c_{12} & \cdots & c_{16} \\ c_{21} & c_{22} & \cdots & c_{26} \\ \vdots & \vdots & \ddots & \vdots \\ c_{61} & c_{62} & \cdots & c_{66} \end{bmatrix}$$

Gravity Vector:

$$G(q) = \begin{bmatrix} g_1 \\ g_2 \\ \vdots \\ g_6 \end{bmatrix}$$

The detailed expressions for each element in these matrices depend on the specific configuration and parameters of the robotic arm. By solving these equations, we can predict the dynamic response of the robotic arm under various conditions, enabling the design of effective control strategies and ensuring the desired performance in practical applications.

3. Simulation Setup

3.1. Modeling the robotic arm

Modeling a 6-DOF robotic arm, specifically the Acrobot from Acrome, in a simulation environment involves a series of systematic steps to ensure an accurate and functional representation. The steps are as follows:

- **Define the Kinematic Structure:** Start by outlining the kinematic configuration using the Denavit-Hartenberg (D-H) parameters. This involves specifying the link lengths, twist angles, offsets, and joint angles for the robotic arm.
- **Build the Geometric Model:** Using a simulation tool such as MATLAB Simulink, create the geometric model of the Acrobot. This involves defining the physical dimensions and properties of each link according to the specifications provided by Acrome.
- **Specify Joint Types and Constraints:** Assign the appropriate joint types (revolute) to each of the

six joints. Define the constraints for each joint, including the range of motion and mechanical limits, to mimic the real-world behavior of the Acrobot.

- **Set Up Coordinate Frames:** Establish coordinate frames for each link and joint based on the D-H parameters. This step is crucial for accurately modeling the kinematic chain of the robotic arm and ensuring proper motion transformations.
- **Incorporate Actuators and Sensors:** Add actuators to drive the joints and sensors to measure joint positions, velocities, and torques. This step is essential for simulating the control and feedback mechanisms of the Acrobot.
- **Define Dynamic Properties:** Input the dynamic properties of the links, such as mass, center of mass, and inertia tensors, based on the provided specifications. These properties are necessary for accurately simulating the forces and torques acting on the robotic arm.
- **Assemble the Complete Model:** Combine all the components (links, joints, actuators, sensors) to create the complete robotic arm model in the simulation environment.

Figure 1 shows the drawing of the 6-DOF robotic arm and the placement of coordinate frames at its joints. Table 1 presents the D-H table for this robotic arm.

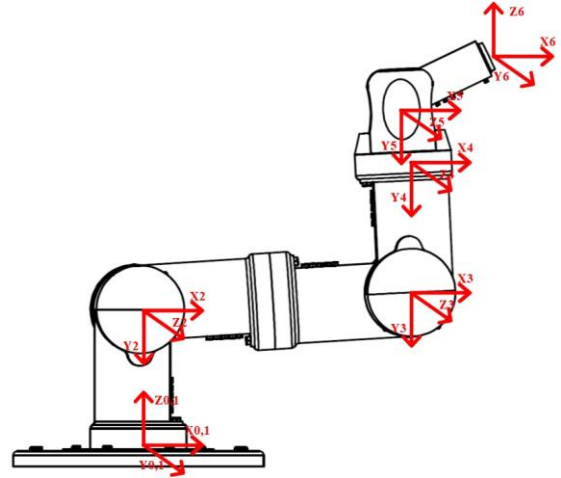


Figure 1. 6 DoF robotic arm with axis

Table 1. Denavit-Hartenberg table of 6 axis industrial robotic arm

Joint (i)	Link Length (a_{i-1}) (m)	Link Twist Angle (α_{i-1}) (degree)	Link Offset (d_i) (m)	Joint Angle (θ_i) (degree)
1.	0	$\pi/2$	0,191	θ_1
2.	0,278	0	0	θ_2
3.	0	$-\pi/2$	0	θ_3
4.	0	$\pi/2$	0,202	θ_4
5.	0	$-\pi/2$	0	θ_5
6.	0	0	0,105	θ_6

To ensure accurate simulation results, it is crucial to define the system parameters and initial conditions

correctly. The following parameters need to be specified: the length and mass of each link according to the specifications of the Acrobot provided by Acrome, the inertia tensors for each link to account for the distribution of mass and rotational dynamics, the range of motion limits for each joint to prevent unrealistic movements during the simulation, and the initial positions and velocities of each joint to represent the starting configuration of the robotic arm. These initial conditions should be set based on the desired starting position of the Acrobot. Additionally, the control gains for the actuators should be set to ensure stable and responsive control of the joints, and these gains may need to be tuned based on the specific control strategy employed. By following these steps and accurately defining the system parameters and initial conditions, a detailed and functional simulation model of the Acrobot can be created. This model will serve as the basis for evaluating the performance of the robotic arm under various operational scenarios and developing effective control strategies.

3.2. Simulation scenarios

The performance and robustness of the 6-DOF Acrobot were evaluated through various simulation scenarios using MATLAB Simulink. These scenarios were designed to replicate real-world conditions and challenges that the robotic arm might encounter. The first scenario involved the robotic arm performing basic joint rotations and translations to verify the accuracy of the kinematic and dynamic models. This scenario was essential for ensuring that the simulation environment accurately represented the physical behavior of the Acrobot. The second scenario focused on path following, where the robotic arm was programmed to follow a predefined trajectory. This scenario was significant for assessing the precision and accuracy of the arm in executing complex tasks such as those required in assembly lines or surgical procedures. Another scenario tested the robotic arm's capability to handle different payloads. By varying the weight of the objects the arm had to manipulate, this scenario helped evaluate the strength and stability of the arm under different load conditions. Additionally, a disturbance rejection scenario was conducted where external forces and torques were introduced to test the robustness and resilience of the control system. This scenario was particularly important for applications in dynamic environments such as space exploration or interaction with humans. Finally, the robotic arm was simulated in a dynamic environment with moving obstacles. This scenario was crucial for testing the arm's adaptability and collision avoidance capabilities, which are vital for safe operation in unpredictable settings.

To effectively simulate these scenarios, appropriate input signals and control strategies were defined and implemented. For the basic joint movements, input

signals were generated to command specific angles and velocities for each joint, allowing the simulation to test the fundamental movements of the robotic arm. In the path-following scenario, a series of waypoints was provided as input signals, guiding the end-effector along a continuous trajectory. These waypoints were converted into joint angle commands through inverse kinematics algorithms. In the payload handling scenario, varying forces were applied to the end-effector to simulate the different weights of objects, and the control system was adjusted to maintain stability and precision under these changing conditions. For the disturbance rejection scenario, external force and torque inputs were introduced at random intervals, and the control strategy focused on compensating for these disturbances to keep the arm on its intended path. In the dynamic environment scenario, input signals included the positions and velocities of moving obstacles, and the control strategy incorporated real-time obstacle detection and avoidance algorithms. This setup ensured that the robotic arm could navigate safely around obstacles while continuing to perform its assigned tasks.

Figure 2 illustrates the simulated 6-DOF robotic arm performing these scenarios. This comprehensive evaluation highlights the Acrobot's capabilities and identifies areas for potential improvement in its design and control systems, ensuring its reliable performance in various applications.

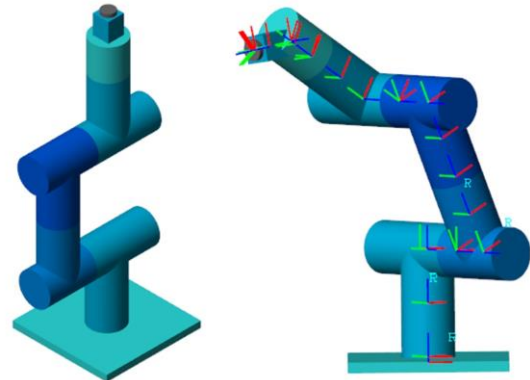


Figure 2. Simulation of 6 DoF robotic arm

Figure 3 illustrates the MATLAB Simulink model of a 6-DoF robotic arm, showcasing a simulation framework where each joint can be individually controlled by providing specific angular position input data. This simulation enables precise control over the robot's motion by allowing tailored inputs for each degree of freedom. The model generates detailed output data for each joint, including angular position, velocity, acceleration, and torque values. These outputs provide a comprehensive understanding of the dynamic behavior of the robotic arm, facilitating the analysis and evaluation of motion control strategies. Such a simulation environment is critical for optimizing system performance, validating theoretical models, and conducting preliminary

testing before deploying the robotic system in real-world applications.

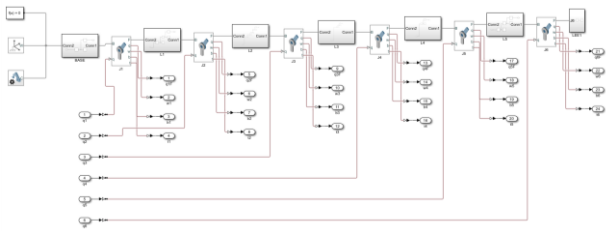


Figure 3. MATLAB simulink model of a 6-DoF robotic arm with individual joint control

Figure 4 presents a detailed MATLAB Simulink model designed for the dynamic analysis of a 6-DoF robotic arm. This model incorporates multiple components to simulate and evaluate the robotic arm's performance under various conditions. The input signal is applied over time, allowing for the generation of desired angular positions, velocities, and accelerations for each joint. The model outputs critical dynamic parameters such as joint positions, velocities, accelerations, and torque values for each joint. Additionally, the configuration includes a forward kinematics block, which calculates the end-effector's XYZ coordinates based on the joint parameters. This allows for precise analysis of the robot's spatial positioning and motion planning. The interconnected blocks ensure that the data flow between inputs and outputs is consistent, providing a robust environment for testing control strategies and validating the robot's dynamic response to various inputs. This simulation serves as a crucial tool in optimizing robotic system designs before physical implementation.

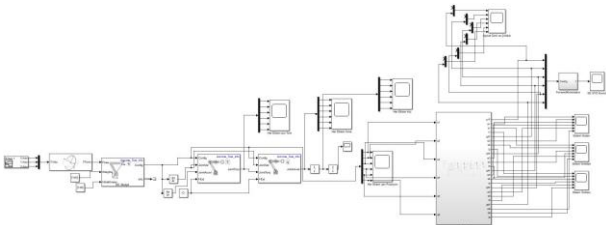


Figure 4. MATLAB simulink model for the dynamic analysis of a 6-DoF robotic arm

4. Results and Discussion

This section presents and examines the simulation results of the dynamic behavior of the 6-DOF robotic arm. The findings are analyzed in terms of angular displacement, velocity, acceleration, and torque profiles for each joint under various operational scenarios. The results offer valuable insights into the performance characteristics of the robotic arm, including its kinematic and dynamic responses, as well as their implications for control strategies and mechanical design. The discussion emphasizes the relevance of these findings in enhancing the robotic arm's functionality for diverse applications.

Figure 5 demonstrates the positional behavior of a 6-DoF robotic arm along the X, Y, and Z axes during a test

simulation. For this test, random position data was generated and applied over a 5-second time interval to evaluate the robotic arm's response. The top plot represents the motion along the X-axis, where the position shows a stepwise increase followed by stability. The middle plot illustrates the Y-axis motion, characterized by an initial increase, a sharp decrease to zero, and subsequent stabilization. The bottom plot depicts the Z-axis position, which gradually increases and remains constant after reaching the desired value. This random input data serves as a test case to observe and analyze the system's ability to track positional changes and maintain stability across all three axes. The results provide insight into the accuracy and reliability of the robotic arm's motion control system.

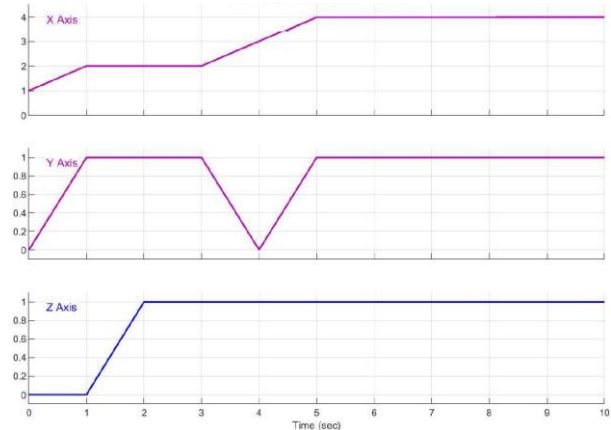


Figure 5. Randomly generated position data for X, Y, and Z axes in a 6-DOF robotic arm test

Figure 6 depicts the joint position profiles for the six degrees of freedom of the robotic arm. The red curves represent the desired joint positions calculated using inverse kinematics equations, while the blue curves illustrate the actual joint positions achieved during the simulation. Notably, significant discrepancies are observed in the first and second joints, indicating a considerable deviation between the desired and achieved positions.

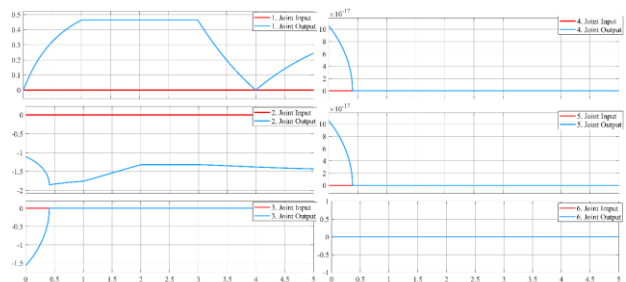


Figure 6. Joint position profiles derived from inverse kinematics (red) and achieved joint positions (blue)

These differences on Figure 6 can primarily be attributed to the random input data provided during the test. The randomness of the inputs may result in configurations where the robot attempts to position its end-effector in areas outside its reachable workspace. Physical constraints such as joint limits, mechanical range of motion, and singularities in the

kinematic structure can prevent the robotic arm from achieving the desired positions. The first joint, responsible for base rotation, and the second joint, controlling the arm's vertical movement, are particularly sensitive to such constraints, as they play critical roles in extending the robot's reach within the workspace. This analysis highlights the importance of ensuring that input data remains within the feasible operational range of the robotic arm. Moreover, it underscores the need for robust kinematic solvers and control systems capable of handling infeasible commands gracefully while maintaining stability. The insights gained from these discrepancies can guide future improvements in motion planning and workspace analysis for robotic systems. The oscillations observed in the initial phase of joint motion suggest transient dynamics associated with the control strategy. These behaviors could potentially be minimized by tuning the parameters of the PID controller, improving overall system stability and response time.

Figure 7 illustrates the joint velocity profiles calculated for the 6-DOF robotic arm to achieve the desired position of the end-effector. Each plot represents the velocity of an individual joint, showcasing significant variations in magnitude and behavior across the joints.

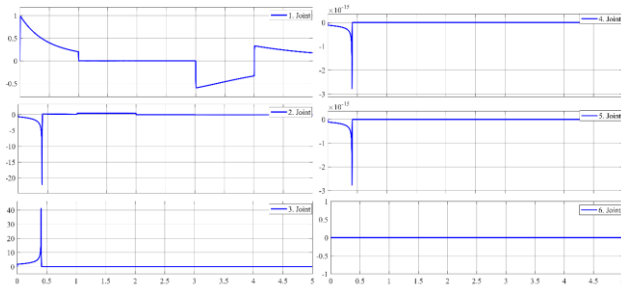


Figure 7. Joint velocities required for reaching the desired end-effector position

The first joint demonstrates relatively high velocity at the initial stage, reflecting the need for rapid rotation of the base to align the robotic arm with the target direction. The second joint exhibits a sharp negative velocity initially, indicative of its role in providing vertical adjustments for the arm to reach the required workspace. The third joint shows an even higher peak velocity compared to the others, which can be attributed to its critical role in extending the arm towards the desired position. The velocities of the wrist joints (joints 4, 5, and 6) are considerably lower and nearly negligible, highlighting their role in fine-tuning the orientation of the end-effector rather than contributing significantly to its spatial positioning. These variations stem from the differing functional responsibilities of each joint in achieving the end-effector's motion. The differences in velocity profiles can be attributed to the distinct mechanical constraints and the kinematic configuration of the robotic arm. The joints closer to the base must handle

broader and larger-scale movements, requiring higher velocities. In contrast, the wrist joints perform precise adjustments, resulting in lower velocities. Additionally, the random nature of the input commands may lead to scenarios where specific joints are required to compensate for others, further amplifying the observed differences. These insights emphasize the importance of joint-specific control strategies to ensure smooth and efficient motion across the robotic arm's range of tasks.

Figure 8 depicts the acceleration profiles for the six joints of the 6-DOF robotic arm, calculated to achieve the desired position of the end-effector. Each plot illustrates the acceleration of an individual joint, showcasing significant variations in magnitude and behavior.

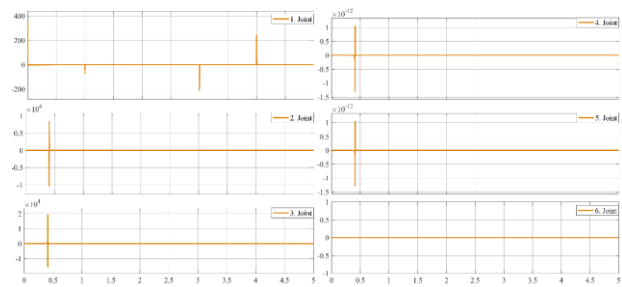


Figure 8. Joint accelerations required for reaching the desired end-effector position

The first joint exhibits the largest acceleration values at the initial stage, reflecting its critical role in generating rapid rotational motion to align the robotic arm toward the target direction. The acceleration drops significantly after the initial adjustment, indicating that further movement requires less effort. Similarly, the second joint demonstrates a sharp initial peak, which corresponds to the necessary vertical adjustment for reaching the target position. The third joint also shows high acceleration values initially, as it contributes to extending the robotic arm towards the target. In contrast, the wrist joints (joints 4, 5, and 6) exhibit minimal acceleration throughout the motion. This is expected, as their primary function is fine-tuning the end-effector's orientation rather than contributing to large-scale positioning. The nearly negligible acceleration values indicate that these joints experience minimal dynamic demands compared to the base and arm joints.

The observed differences in acceleration can be attributed to the kinematic roles of the joints and the random nature of the input commands. Base and arm joints (joints 1, 2, and 3) are responsible for broader and more force-intensive movements, requiring higher accelerations, especially during the initial stages of motion. In contrast, the wrist joints primarily perform precise adjustments with minimal dynamic demands. These insights highlight the need for tailored control strategies that account for the specific

dynamic requirements of each joint, ensuring efficient and stable operation.

Figure 9 illustrates the torque profiles for the six joints of the 6-DOF robotic arm, calculated to achieve the desired position of the end-effector under a no-load condition. Each graph highlights the torque demand of a specific joint, revealing significant variations in magnitude and behavior across the joints.

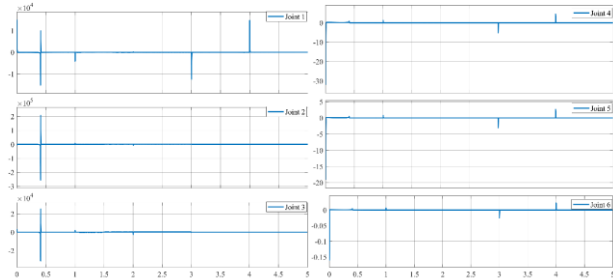


Figure 9. Joint torques required for reaching the desired end-effector position

The first joint exhibits the highest torque spikes initially, reflecting its role in rotating the base to align the arm with the target direction. This high demand corresponds to overcoming the inertia of the arm and any initial static friction. The second joint displays the largest sustained torque values during motion, as it supports vertical adjustments and bears the arm's weight. The third joint also shows considerable torque requirements, especially during extension motions, as it contributes to positioning the arm closer to the target. In contrast, the wrist joints (joints 4, 5, and 6) require significantly lower torques throughout the motion. Their primary function is to finely adjust the orientation of the end-effector, which involves minimal resistance compared to the broader motions of the base and arm joints.

These torques were calculated under no-load conditions, meaning the values represent only the arm's inherent weight and mechanical constraints. For instance, the first joint's peak torque under these conditions is approximately $1.2 \times 10^4 Nm$, while the second joint reaches around $2 \times 10^5 Nm$. These values would increase significantly with added payloads, depending on the load distribution and the robot's configuration. Given the results, the motors selected for each joint must be capable of handling these baseline torques and any additional demand introduced by payloads. For example, if a payload of 5 kg is added at the end-effector, the second joint torque could rise by an estimated 20-30%, requiring a motor with a higher torque tolerance. Similarly, the first joint's torque might increase by 10-15% due to the extended leverage effect.

It is essential to ensure that the torque capacity of the motors includes a safety margin to accommodate these variations. This will guarantee reliable performance and prevent mechanical failures.

Additionally, the torque limitations imposed by the arm's no-load weight and the kinematic constraints must be considered when designing and selecting actuators, ensuring that the robotic arm can operate effectively across its entire workspace under various load conditions. The high torque demands observed in the base joint indicate the need for a more robust actuator with higher torque capacity. This directly impacts motor selection and power requirements, especially in applications where the arm must operate under varying payloads or continuous duty cycles.

Figure 10 illustrates the final output positions of the robotic arm's end-effector along the X, Y, and Z axes over a 5-second interval. The red, blue, and yellow lines represent the X, Y, and Z axis outputs, respectively. These outputs are the results of the robotic arm's movement to achieve the desired end-effector position, as calculated by the inverse kinematics and implemented through joint control.

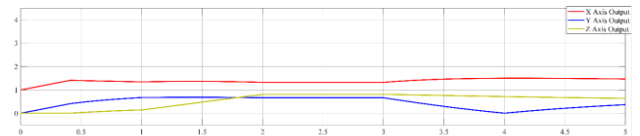


Figure 10. Final end-effector position of the robotic arm along X, Y, and Z axes

Compared to the initial input positions provided earlier, deviations are observed between the desired inputs and the final outputs, particularly along the Y and Z axes. While the X-axis output closely follows the input trajectory with minor deviations, the Y-axis exhibits noticeable oscillations, and the Z-axis deviates slightly from the desired position. These discrepancies can be attributed to the physical constraints of the robotic arm, including joint limitations, mechanical inaccuracies, and the dynamic interactions between joints during motion.

The differences highlight the importance of calibrating the control system to minimize errors and improve positional accuracy. Such adjustments are critical for ensuring that the robotic arm performs tasks requiring precise spatial positioning. Despite these deviations, the overall trajectory demonstrates the arm's capability to approximate the desired positions effectively under the given conditions. Further optimization of control algorithms and actuator responses may enhance the accuracy of the end-effector's final positioning in future iterations. The results obtained from the dynamic simulation of the 6-DOF robotic arm align with findings in existing literature. For instance, dynamic simulations have shown that the base and shoulder joints experience higher torque demands due to their structural load-bearing roles and extensive range of motion [34], which is consistent with the observations in this study. Additionally, the wrist joints exhibit lower torque and acceleration values, reflecting their primary function in fine orientation adjustments rather than significant

load-bearing. Furthermore, deviations between desired and actual end-effector positions, particularly under varying input conditions, are often attributed to kinematic singularities and joint limitations, as discussed in the literature [35, 36]. These parallels reinforce the validity of the simulation approach and underscore the relevance of the findings to practical robotic applications.

5. Conclusion

This study conducted a comprehensive dynamic analysis of a 6-DOF robotic arm using advanced simulation techniques in MATLAB Simulink. The results provided valuable insights into the robotic arm's performance across a range of operational scenarios, including angular displacement, velocity, acceleration, and torque profiles for each joint. The analysis revealed distinct dynamic roles for each joint, providing critical data for control system optimization and mechanical design. The analysis highlighted the distinct functional roles and dynamic demands of each joint, emphasizing the necessity of joint-specific control strategies and actuator designs.

Key findings revealed that the base joint requires the largest angular displacements and torques due to its role in broad rotational movements, while the wrist joints, responsible for precise adjustments, exhibited smaller but more frequent peaks in velocity and acceleration. These observations underscore the need for robust control systems capable of addressing both large-scale positioning and fine-tuned adjustments. The simulation scenarios, which included basic joint movements, path following, payload handling, disturbance rejection, and dynamic navigation, demonstrated the robotic arm's adaptability and precision in handling diverse tasks. The results validate the potential of the 6-DOF robotic arm for applications in fields such as manufacturing, medical surgeries, and space exploration.

This research contributes to the optimization of 6-DOF robotic arm design and control. The torque and dynamic response profiles presented serve as benchmarks for future developments, aiding engineers in enhancing the efficiency, reliability, and adaptability of robotic systems. Future work should focus on refining control algorithms, exploring the use of advanced materials, and integrating adaptive learning mechanisms to further improve performance under real-world conditions. The most significant finding of this study is the identification of joint-specific torque demands, which can inform actuator selection and control system development in advanced robotic applications.

References

- [1] Moran, M.E., Evolution of robotic arms. *Journal of robotic surgery*, 2007. 1(2): p. 103-111.
- [2] Kruthika, K., B.K. Kumar, and S. Lakshminarayanan. Design and development of a robotic arm. in *2016 International Conference on Circuits, Controls, Communications and Computing (I4C)*. 2016. IEEE.
- [3] Camarillo, D.B., T.M. Krummel, and J.K. Salisbury Jr, *Robotic technology in surgery: past, present, and future*. The American Journal of Surgery, 2004. 188(4): p. 2-15.
- [4] FreeDman, D., *Robotic*. 1991.
- [5] Murray, R.M., Z. Li, and S.S. Sastry, *A mathematical introduction to robotic manipulation*. 2017: CRC press.
- [6] Kucuk, S. and Z. Bingul, *Robot kinematics: Forward and inverse kinematics*. 2006: INTECH Open Access Publisher London, UK.
- [7] Waldron, K.J. and J. Schiedeler, *Kinematics*. Springer handbook of robotics, 2016: p. 11-36.
- [8] Featherstone, R. and D. Orin. Robot dynamics: equations and algorithms. in *Proceedings 2000 ICRA. Millennium conference. IEEE international conference on robotics and automation. Symposia proceedings (Cat. No. 00CH37065)*. 2000. IEEE.
- [9] Lilly, K., *Efficient dynamic simulation of robotic mechanisms*. Vol. 203. 2012: Springer Science & Business Media.
- [10] Farman, M., M. Al-Shaibah, Z. Aoraiath, and F. Jarrar, Design of a three degrees of freedom robotic arm. *International Journal of Computer Applications*, 2018. 179(37): p. 12-17.
- [11] Kubalak, J.R., et al., Design and realization of a 6 degree of freedom robotic extrusion platform. 2016.
- [12] Huo, Z., M. Yuan, S. Zhang, and X. Zhang. Observer-Based Adaptive Robust Force Control of a Robotic Manipulator Integrated with External Force/Torque Sensor. in *Actuators*. 2025. MDPI.
- [13] Hayat, A.A., R.G. Chittawadigi, A.D. Udai, and S.K. Saha. Identification of Denavit-Hartenberg parameters of an industrial robot. in *Proceedings of conference on advances in robotics*. 2013.
- [14] Rocha, C., C. Tonetto, and A. Dias, A comparison between the Denavit-Hartenberg and the screw-based methods used in kinematic modeling of robot manipulators. *Robotics and Computer-Integrated Manufacturing*, 2011. 27(4): p. 723-728.
- [15] Granja, M., et al. Comparison between standard and modified denavit-hartenberg methods in robotics modelling. in *Proceedings of the 2nd World Congress on Mechanical, Chemical, and Material Engineering (MCM'16) Budapest, Hungary*. 2016.

- [16] Kurdila, A.J. and P. Ben-Tzvi, Dynamics and control of robotic systems. 2019.
- [17] Spong, M.W. and M. Vidyasagar, Robot dynamics and control. 2008: John Wiley & Sons.
- [18] Tchoń, K. and J. Ratajczak, General Lagrange-type Jacobian inverse for nonholonomic robotic systems. *IEEE Transactions on Robotics*, 2017. 34(1): p. 256-263.
- [19] Li, X., X. Wang, and J. Wang, A kind of lagrange dynamic simplified modeling method for multi-DOF robot 1. *Journal of Intelligent & Fuzzy Systems*, 2016. 31(4): p. 2393-2401.
- [20] De Luca, A. and L. Ferrajoli. A modified Newton-Euler method for dynamic computations in robot fault detection and control. in 2009 IEEE International Conference on Robotics and Automation. 2009. IEEE.
- [21] Hwang, Y.-L., Recursive Newton-Euler formulation for flexible dynamic manufacturing analysis of open-loop robotic systems. *The International Journal of Advanced Manufacturing Technology*, 2006. 29: p. 598-604.
- [22] Iqbal, J., R.U. Islam, and H. Khan, Modeling and analysis of a 6 DOF robotic arm manipulator. *Canadian Journal on Electrical and Electronics Engineering*, 2012. 3(6): p. 300-306.
- [23] Pratheep, V., et al. Design and Analysis of six DOF robotic manipulator. in *IOP Conference Series: Materials Science and Engineering*. 2021. IOP Publishing.
- [24] Aghili, F. and K. Parsa. A robot with adjustable dh parameters. in 2007 International Conference on Mechatronics and Automation. 2007. IEEE.
- [25] Zhang, T., Y. Song, H. Wu, and Q. Wang, A novel method to identify DH parameters of the rigid serial-link robot based on a geometry model. *Industrial Robot: the international journal of robotics research and application*, 2021. 48(1): p. 157-167.
- [26] Natale, C. and M. Gandhi, Interaction control of robot manipulators: six degrees-of-freedom tasks. *Appl. Mech. Rev.*, 2004. 57(2): p. B10-B10.
- [27] Kobayashi, Y., et al., Development of a robotic system with six-degrees-of-freedom robotic tool manipulators for single-port surgery. *The International Journal of Medical Robotics and Computer Assisted Surgery*, 2015. 11(2): p. 235-246.
- [28] Shafei, A. and H. Shafei, Dynamic modeling of tree-type robotic systems by combining 3×3 rotation and 4×4 transformation matrices. *Multibody System Dynamics*, 2018. 44(4): p. 367-395.
- [29] Salvietti, G., M. Malvezzi, G. Gioioso, and D. Prattichizzo. On the use of homogeneous transformations to map human hand movements onto robotic hands. in 2014 IEEE International Conference on Robotics and Automation (ICRA). 2014. IEEE.
- [30] Falkenhahn, V., et al., Dynamic modeling of bellows-actuated continuum robots using the Euler-Lagrange formalism. *IEEE Transactions on Robotics*, 2015. 31(6): p. 1483-1496.
- [31] Jain, A. and G. Rodriguez, Diagonalized Lagrangian robot dynamics. *IEEE Transactions on Robotics and Automation*, 1995. 11(4): p. 571-584.
- [32] Stroe, I., S. Staicu, and A. Craifaleanu. Internal forces calculus of compass robotic arm using Lagrange equations. in 10th ESA Workshop on Advanced Space Technologies for Robotics and Automation 'ASTRA. 2011.
- [33] Sharkawy, A.-N., Impact of Inertial and External Forces on Joint Dynamics of Robotic Manipulator: Experimental Insights. *Control Systems and Optimization Letters*, 2025. 3(1): p. 1-7.
- [34] New, K. and W.P. Maung, Dynamic Simulation And Motion Load Analysis Of Six DOF Articulated Robotic Arm. *International Journal of Mechanical and Production Engineering*, 2018. 6(5): p. 13-17.
- [35] Shamir, T., The singularities of redundant robot arms. *The International journal of robotics research*, 1990. 9(1): p. 113-121.
- [36] Remis, S.J. and M.M. Stanisic, Design of a singularity-free articulated arm subassembly. *IEEE transactions on robotics and automation*, 1993. 9(6): p. 816-824.